



# Stress state of the northwest Indian shield with emphasis on the Intraplate Delhi Seismic Zone

A MANGLIK\*, G PAVANKUMAR and M DEMUDU BABU

CSIR-National Geophysical Research Institute, Uppal Road, Hyderabad 500 007, India.

\*Corresponding author. e-mail: ajay@ngri.res.in amngri@gmail.com

MS received 21 June 2022; revised 26 November 2022; accepted 29 November 2022

The northwest Indian shield is seismically moderately active with frequent occurrence of small–moderate magnitude earthquakes. These earthquakes occur mainly along the NE–SW oriented Proterozoic Aravalli–Delhi Fold Belt (ADFB) and along another NNW–NW trending tectonic feature from Delhi westward, the inferred Delhi–Sargodha Ridge (DSR). The Delhi Seismic Zone (DSZ) falls in the region of the DSR and is about 200–250 km south of the Himalayan front. Thus, the DSZ region seems to be experiencing stresses both of intraplate and plate boundary nature. In order to understand the role of ADFB and the DSR in generating the intraplate stresses, we have carried out elastostatic stress modelling to estimate the intraplate stresses for the region. We analyze these stresses in conjunction with the regional compressive plate tectonic stress and the bending stresses due to flexure of the Indian plate. The results reveal dominantly strike-slip-type focal mechanisms for the ADFB, but the stress state is relatively complex for the DSZ. Here, the bending stresses lead to a dominant strike-slip-type environment at shallow levels (<10 km) and a thrust-type environment at deep levels (>20 km). A comparison of these results with the earthquake focal mechanisms suggests that intraplate stresses modulated by plate bending stresses are needed to explain the seismicity of the DSZ, implying a coupling between the local stresses and those induced by the Himalayan loading. The results suggest inclusion of plate bending stresses in earthquake hazard assessment models of the DSZ and the northwest Indian shield.

**Keywords.** Intraplate seismicity; stress; Indian shield; Himalaya.

## 1. Introduction

Seismicity within plate interior, through infrequent accounting for only 0.5% of the global strain energy release (Johnson and Kanter 1990), is enigmatic and challenging for earthquake hazard assessment due to slow rate of strain energy accumulation and seismic loading. Several causative mechanism have been suggested to explain intraplate seismicity, e.g., reactivation of ancient failed rifts and modulation of plate tectonic stresses by local preexisting

weak zones (Sykes 1978; Braile *et al.* 1982; Johnston and Kanter 1990), surface and subsurface loading due to topography load and crustal heterogeneities (Mareschal and Kuang 1986; Kuang *et al.* 1989; Mandal *et al.* 1993, 1997), dynamic uplift and extensional stresses by a mantle plume (Cox 1989), glacial isostatic adjustment (Muir-Wood 2000; Mazzotti *et al.* 2005; Keiding *et al.* 2015), and reservoir loading and triggering (Carder 1945; Simpson 1976). These hypotheses treat intraplate regions as isolated from the plate

Supplementary materials pertaining to this article are available on the *Journal of Earth System Science* website ([http://www.ias.ac.in/Journals/Journal\\_of\\_Earth\\_System\\_Science](http://www.ias.ac.in/Journals/Journal_of_Earth_System_Science)).

Published online: 28 March 2023

boundary effects except in some cases in which regional stresses induced by plate boundary forces are added to the local stresses to get the resultant stress state (e.g., Kuang *et al.* 1989; Mandal *et al.* 1997). Such models may not be applicable to the intraplate regions located about 200–400 km away from a collision front for typical values of flexural rigidity of the lithosphere as the bending stresses due to plate flexure can be significantly large up to the flexural bulge at  $0.75\pi$  (infinite beam) to  $\pi$  (finite beam) times the flexural wavelength (Watts 2001) and can contribute significantly large stress to the total stress state of such intraplate regions.

The Delhi Seismic Zone (DSZ) (figure 1) in northwest India is one such seismically active intraplate region that is located about 200–250 km

south of the Himalayan frontal belt. This region, encompassing the National Capital Region of Delhi (Delhi–NCR) and some neighbouring regions, is considered to be one of the most seismically active intraplate regions in the Indian shield. The DSZ falls in the Seismic Zone IV of the Seismic Zoning Map of India (BIS IS 1893, Part 1: 2002). Seismicity in this region is minor–moderate in nature, though the largest event reported in recent times is the 27 August 1960 earthquake ( $M 6.0$ ) with the epicentre between Delhi and Gurgaon (Iyengar 2000). There have been many minor earthquakes and a moderate magnitude earthquake ( $M 4.5$ ) during the year 2020 (<https://riseq.seismo.gov.in/riseq/earthquake/archive>). The DSZ seismicity is attributed to some of the major tectonic features

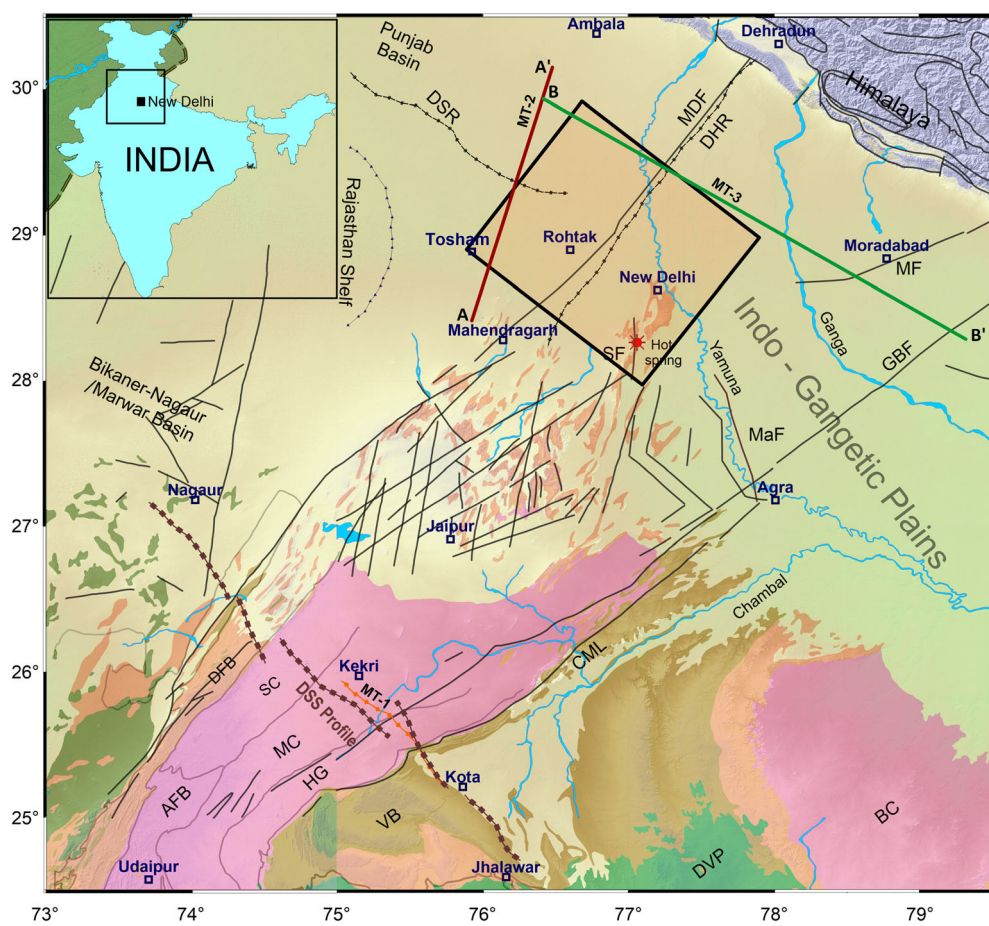


Figure 1. Map showing major geological and tectonic features in the NW Indian shield. The DSZ is marked by a rectangle covering Delhi and Rohtak. The MT profiles across the DSR (MT-2) and the MDF/DHR (MT-3), and the Nagaur–Jhalawar DSS profile and Kekri–Kota MT profile (MT-1) are also marked. Inset shows the location of the region on the map of India. Figure modified after Pavankumar *et al.* (2021) in which major geological and structural features shown in the figure were taken from the shape files available at the BHUKOSH portal of Geological Survey of India (<http://bhukosh.gsi.gov.in/Bhukosh/MapView.aspx>) and geological domains and faults of the ADFB were from Tiwari *et al.* (1997). Abbreviations in the map are – AFB: Aravalli Fold Belt, SC: Sandmata Complex, MC: Mangalwar Complex, HG: Hingoli Group, DFB: Delhi Fold Belt, VB: Vindhyan Basin, DVP: Deccan Volcanic Province, BC: Bundelkhand Craton, DHR: Delhi–Haridwar Ridge, DSR: Delhi–Sar-godha Ridge, GBF: Great Boundary Fault, SF: Sohna Fault, MDF: Mahendragarh–Dehradun Fault, MaF: Mathura Fault, MF: Moradabad Fault, and CML: Chittaurgarh–Machilpur lineament.

such as the Aravalli–Delhi Fold Belt (ADFB), the Delhi–Sargodha Ridge (DSR), and some inferred faults, e.g., the Mahendragarh–Dehradun Fault (MDF) (figure 1) (Shukla *et al.* 2007). The ADFB is a long linear NE–SW trending structure of topography and Bouguer gravity high extending over a length of about 700 km in NW India. The DSR does not have surface expressions but has been inferred as a NW trending feature between Delhi and Sargodha/Lahore (Rao 1973). Similarly, the MDF is also not exposed and has been inferred. There have been several earthquakes along the entire length of the ADFB, but the seismicity around Delhi has been attributed mainly to the inferred DSR and the MDF.

The DSZ being in the proximity of the Himalayan collision belt and at the juncture where the Indian plate starts flexing due to the mountain load, large plate bending stresses are expected to have a major contribution to the stress state of this region as well as the entire northern part of the Indian shield. There are several studies using gravity anomaly and elevation profiles across the Indian shield and the Himalaya to estimate the flexural rigidity and elastic thickness of the Indian plate and their variations along the Himalayan arc (e.g., Karner and Watts 1983; Lyon-Caen and Molnar 1983, 1985; Jordan and Watts 2005; Hetényi *et al.* 2006). These estimates of flexural rigidity and wavelength can be used to calculate the plate bending stresses in the NW Indian shield, including the DSZ. In the present work, we calculate local elastostatic stresses due to topography and heterogeneities in the crustal density and mechanical properties and plate bending stresses due to the flexure of the Indian plate. We then analyze these stresses in conjunction with the estimates of the regional plate tectonic compressive stress and the prevailing seismicity of the NW Indian shield, especially the DSZ, to develop a model of the stress state of the region.

## 2. Geology and tectonics

The geology of the northwest Indian shield is dominated by a long linear trend of fold belts of early–middle Proterozoic age overlying the Archaean gneissic basement, together known as the Aravalli–Delhi Fold Belt (Roy 1988; Sinha-Roy *et al.* 1995). This belt extends from south of Udaipur up to Delhi in NE–SW direction and covers a length of about 700 km (figure 1). At

Delhi, it gets buried under the alluvial sediments of the Indo-Gangetic Plains. Its further northward continuation beneath the alluvial cover of the Indo-Gangetic Plains and the Lesser Himalaya as the Delhi–Haridwar Ridge has been inferred from geomagnetic depth sounding studies (Lilley *et al.* 1981; Arora and Mahashabde 1987). However, in recent years an alternative view based on gravity modelling has suggested that the ADFB takes a northwest turn at Delhi and continues westward as the DSR (Dwivedi *et al.* 2019). The DSZ falls in this region where the surface exposures of the ADFB start disappearing. The Marwar Basin and the Rajasthan shelf mark the western boundary of the ADFB, whereas the Vindhyan Basin forms its NE boundary (figure 1). The term ADFB collectively represents the Aravalli Fold Belt, the Delhi Fold Belt, and the Sandmata Complex, the Mangalwar Complex and the Hindoli Group of the Bhilwara Supergroup comprising the basement gneissic complex (Sinha-Roy *et al.* 1995). The Aravalli Fold Belt, exposed in the SW part of the belt (figure 1), is of early Proterozoic age (~2.5–2.0 Ga). It is bounded on the west by the Delhi Fold Belt of middle Proterozoic age (~2.0–1.5 Ga) that is exposed till the northern extent of the exposed ADFB and is subdivided into the north Delhi Fold Belt and the south Delhi Fold Belt.

Tectonically, the eastern limit of the ADFB is marked by a prominent dislocation boundary, known as the Great Boundary Fault (GBF), between the Hindoli Group and the Proterozoic Vindhyan Supergroup. The western boundary of the ADFB separates the exposed Delhi Fold Belt from the Marwar basin. It is assumed to be continuing beneath the Indo-Gangetic Plains as the Delhi–Haridwar Ridge (DHR) or as the Mahendragarh–Dehradun Fault (MDF) (also named as the Mahendragarh–Dehradun Subsurface Fault (MDSSF) in literature (Shukla *et al.* 2007). There are many lineaments and faults within the ADFB (figure 1), some of which, such as the Sohna Fault, have also been linked to the seismicity of the DSZ (Prakash and Shrivastava 2012). Besides ADFB, the NW–SE trending DSR is considered as an important tectonic feature in the NW Indian shield although it has no surface manifestation except a few isolated outcrops of the Aravalli rocks near Tosham in Punjab (Rao 1973) and a linear NW–SE trend of the Bouguer gravity high along the axis of the inferred DSR (GSI-NGRI 2006). Recent magnetotelluric (MT) study has revealed the presence

of a north-dipping crustal conductor whose surface location coincides with the axis of the DSR (Pavankumar *et al.* 2021).

## 2.1 Crustal structure

Although very little information is available about the crustal structure of the DSZ where the ADFB gets buried beneath the alluvial cover, the crustal structure of the ADFB has been mapped in detail along the Nagaur–Jhalawar geo-transect (figure 1) by integrated geophysical and geological studies. These studies used deep seismic sounding (DSS), gravity, magnetotelluric, and deep resistivity sounding methods. Some of the major results obtained about the crustal structure of the ADFB include identification of a crustal-scale thrust, named as the Jahazpur thrust, separating the Mangalwar Complex and the Hindoli group (figure 1) and a dome-shaped intrusive structure in the mid-lower crust beneath the Delhi Fold Belt (Tewari *et al.* 1997). Gravity study (Mishra *et al.* 2000) further suggested high density ( $3.04 \text{ g/cm}^3$ ) for the dome-shaped body in the lower crust and linked this to an underplated lower crust caused by extension during the evolution of the Proterozoic rifts. MT study (Gokarn *et al.* 1995) covered only a segment of the Nagaur–Jhalawar profile between Kekri and Kota (figure 1) to map the geoelectric characteristics of the Jahazpur thrust. In view of moderate seismicity associated with the ADFB, Manglik *et al.* (2009) analyzed the role of these major crustal heterogeneities in the generation of intraplate stresses through finite element modelling. Recently, Dwivedi *et al.* (2019) performed a 3-D structural inversion of the Bouguer gravity data and derived a model of the crustal structure of the DSZ region along the axis of the DSR. In this model, the Moho is at 40 km depth with an upwarp, similar to that mapped along the Nagaur–Jhalawar geotransect but of smaller amplitude, beneath the Delhi Fold Belt and the crust below 8 km depth has high-density values, similar to that of a continental lower crust.

North of Delhi, where the ADFB is not exposed on surface, very little information is available on its exact disposition and crustal structure. Lilley *et al.* (1981) analyzed geomagnetic depth sounding array data from NW India and postulated a NE–SW striking line of strong current flow towards the ADFB. The strength of this current was stronger at the Himalayan front rather than at the ADFB.

They attributed this current flow to the presence of an electrical conductor deep in the crust or upper mantle and inferred this to be the northward continuation of the ADFB. Arora and Mahashabde (1987) modelled the magnetic induction vectors for the sites along the Himalayan arc in the Lesser Himalaya and explained the anomalous magnetic field in terms of a 45-km wide electrical conductor reaching to the depth of 15 km from the asthenospheric levels. Arora (1993) synthesized the results of this trans-Himalayan conductor and some other conductors in NW India and remodelled the data. The new model revealed an anticline-shaped conductor of 10–15 km thickness in the 10–30 km depth beneath the Lesser Himalaya, correlating with the northward projection of the ADFB beneath this region. In a recent study, Pavankumar *et al.* (2021) delineated a northward dipping electrical conductor coinciding with the surface location of the DSR and reaching down to 20–25 km depth (profile MT-2 in figure 1). The spatial and depth distribution of the seismicity in the western part of the DSZ coincides with this conductor. The latest results on the northward continuation of the concealed ADFB are by Manglik *et al.* (2022a), who have delineated the detailed subsurface expressions of the ADFB beneath the alluvial cover of the Ganga Basin north of the DSZ through a MT study along a profile-cutting across the inferred location of the ADFB (profile MT-3 in figure 1). Their results reveal that the concealed ADFB consists of a collage of nearly vertical conductive and resistive blocks buried beneath about 1–1.3 km thick alluvial sediments. The boundaries of major inferred tectonic features, such as the western boundary of the DHR and the GBF, as well as the locations of the Ganga and the Yamuna rivers coincide with such steep contacts.

## 3. Seismicity distribution

The NW Indian shield is moderately seismically active and most of the seismicity outside the DSZ is associated with the ADFB. Figure 2 presents a seismicity map of the region, which has been prepared by using the earthquake data ( $M \geq 3$ ) of the entire region during 2000–April 2020 from the ISC catalogue (<http://www.isc.ac.uk/iscbulletin/search/catalogue/>). For the DSZ region, we have also plotted smaller magnitude earthquakes ( $2 \leq M < 3$ ) during this period from a seismic network of National Seismological Centre (NCS),

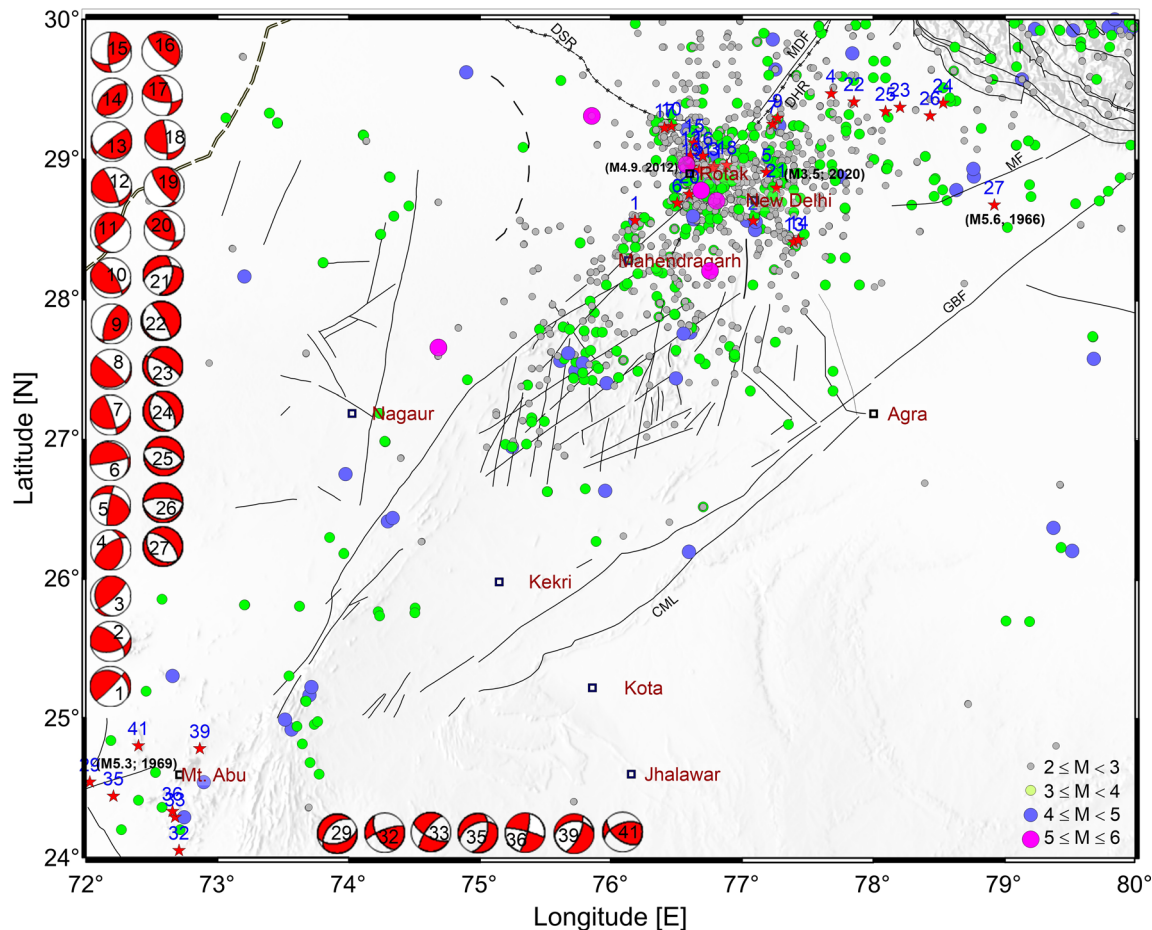


Figure 2. Distribution of the seismicity during 2000–April 2020 in the ADFB region of western India. The data of ( $M \geq 3$ ) events are taken from the ISC catalogue (<http://www.isc.ac.uk/iscbulletin/search/catalogue/>). For the DSZ, events of ( $2 \leq M < 3$ ) have also been included from the catalogue of National Seismological Centre (NCS), Ministry of Earth Sciences (MoES), India (<https://riseq.seismo.gov.in/riseq/earthquake/archive>). Focal mechanisms have been compiled from published literature and provided as supporting information (table S1). Major lineaments and faults are the same as in figure 1.

Ministry of Earth Sciences (MoES), India (<https://riseq.seismo.gov.in/riseq/earthquake/archive>) operated around Delhi. We have also compiled published focal mechanism solutions (table S1, supporting information) and plotted these earthquakes in figure 2 along with the focal mechanism solutions. A large concentration of small magnitude events in the DSZ and surrounding region is mainly attributed to the availability of a local seismic network in that region to monitor the seismicity of the Delhi region. However, relatively large number of earthquakes, albeit of small magnitude, could also be linked to the stress concentration at the junction of orthogonal ADFB and the DSR. From the focal mechanisms, it can be seen that majority of the earthquakes are of strike-slip nature, which can be explained in terms of slip along some faults of the ADFB that are favourably oriented to the N–NNE directed compressive plate tectonic stresses (Gowd *et al.* 1992). However, many events in the DSZ and the Ganga

Basin also have thrust- and normal-faulting dominated focal mechanisms.

Since our focus is to study the stress state and seismicity of the northwest Indian shield with an emphasis on the DSZ, where plate bending stresses can have a significant contribution to the stress state, we discuss the seismic studies carried out for this region in some detail. Some early work focused on seismic monitoring of the region, e.g., in 1963–1964 (Kamble and Chaudhary 1979) and during 1990–1994 (Chauhan *et al.* 1998). Shukla *et al.* (2007) analyzed focal mechanisms of 19 events in the region and suggested a compressional regime for the region with thrust faulting as the dominant fault mechanism with minor strike-slip components. The strike directions of fault planes of many of these events align with the trend of the DSR, and dip angles suggest a steep dip. These earthquakes, which do not appear to be directly associated with the ADFB have been linked to

some other postulated faults, e.g., the MDF that is believed to be a major buried fault extending from Mahendragarh up to the Himalayan foothills and the Sohna Fault west of Delhi along which a hot spring is located at Sohna (figure 1). Prakash and Shrivastava (2012) reviewed the seismotectonics of Delhi and surrounding regions and suggested an active role of the MDF and the DSR for the seismicity activity of the DSZ.

## 4. Mathematical formulation

### 4.1 Local stresses due to crustal heterogeneities and topography

For local stress computations, here we briefly mention the mathematical formulation of Kuang *et al.* (1989), which was used by Mandal *et al.* (1997) to compute intraplate stresses for the Latur intraplate earthquake region. In this formulation, the lithosphere is considered to be constituted of  $N - 1$  elastic layers representing the crust and the mantle lithosphere (figure S1, supplementary information). These layers are assumed to be horizontal with undulations superimposed to create the density and the Bouguer gravity anomalies. The lithosphere rests on an inviscid half-sphere, i.e., the asthenosphere.

The stress tensor ( $\bar{\sigma}$ ) satisfies

$$\nabla \cdot \bar{\sigma} = -\rho \bar{g}, \quad (1)$$

where  $\rho$  and  $\bar{g}$  are the density of the medium and the gravity acceleration, respectively. Following the Hooke's law, the stress for an elastic isotropic medium is related to the strain and hence the displacement as follows:

$$\bar{\sigma} = \lambda(\nabla \cdot \bar{u})\bar{I} + \mu(\nabla \bar{u} + \nabla \bar{u}^T), \quad (2)$$

where  $\bar{u}$  is the displacement vector,  $\bar{I}$  is the identity matrix, and  $\lambda$ , and  $\mu$  are the Lame's parameters. By applying the boundary conditions at the free surface ( $z = h^0 = 0$ )

$$\sigma_{xz}^1 = \sigma_{yz}^1 = 0, \quad \sigma_{zz}^1 = \rho^1 g u_z^1 - P^1, \quad (3a)$$

and at the base of the lithosphere ( $z = h^{N-1} = H$ )

$$\sigma_{xz}^{N-1} = \sigma_{yz}^{N-1} = 0, \quad -\sigma_{zz}^{N-1} = (\rho^N - \rho^{N-1}) g u_z^{N-1}, \quad (3b)$$

and interface conditions ( $z = h^i; i = 1, \dots, N - 2$ )

$$\bar{u}^i = \bar{u}^{i+1}, \quad (4a)$$

$$\begin{aligned} \sigma_{xz}^i &= \sigma_{yz}^{i+1}, \quad \sigma_{yz}^i = \sigma_{yz}^{i+1}, \\ \sigma_{zz}^i &= \sigma_{zz}^{i+1} - (\rho^{i+1} - \rho^i) g u_z^i - P^i, \end{aligned} \quad (4b)$$

the solution of equation (1) can be obtained in the Fourier transform domain as:

$$\bar{u} = A e^{kz} + C e^{-kz}. \quad (5)$$

Here,  $P^i$  is the internal load at the  $i$ th interface. The coefficients  $A$  and  $B$  have three components, each corresponding to the Cartesian coordinate system, and thus, the problem reduces to solving matrix for six unknowns for every layer for the prescribed boundary and interface conditions. Once the displacement vector is known in the Fourier transform domain, the inverse Fourier transform is performed to get the solution in the spatial domain. From the known displacement, stress components can be computed using equation (2).

### 4.2 Bending stresses due to plate flexure

Flexure of the Indian plate due to the Himalayan load has been quantitatively explained in terms of a semi-infinite plate model in which topography load was applied at one end of the plate (Karner and Watts 1983; Lyon-Caen and Molnar 1983, 1985; Jordan and Watts 2005). Flexure of a semi-infinite elastic plate as a function of distance  $x$  due to load  $P_0$  at  $x = 0$  (figure S2, supplementary information) is expressed in mathematical form as (Watts 2001):

$$y = \frac{2P_0\lambda}{(\rho_m - \rho_s)g} e^{-\lambda x} \cos \lambda x$$

or

$$y = y_0 e^{-\lambda x} \cos \lambda x, \quad (6)$$

where  $y$  is the subsidence along the plate, i.e., along the  $x$ -direction and  $y_0$  is the maximum subsidence.  $\lambda$ ,  $\rho_m$ ,  $\rho_s$ , and  $g$  are the flexural wavenumber, density of the mantle lithosphere, density of infilled sediments, and acceleration due to gravity, respectively.

In equation (6), subsidence  $y$  is zero at  $x = \pi/2\lambda, 3\pi/2\lambda, \dots$ . Flexural wavenumber is related to the flexural rigidity  $D$ , and hence the thickness of the elastic plate  $T_e$ , by the following expressions

$$\lambda = \left( \frac{(\rho_m - \rho_s)g}{4D} \right)^{1/4}, \quad D = \frac{ET_e^3}{12(1-v^2)}, \quad (7)$$

where  $E$  and  $v$  are Young's modulus and Poisson's ratio, respectively.

Equation (6) can be used to calculate flexural subsidence at any point along the  $x$ -axis. In actual geophysical problems, this requires information on the actual geographical location of the origin of the coordinate system, which in actual practice is not known. However, geographical location of the first node  $x_s = \pi/2\lambda$  (figure S2, supplementary information) can be found from the Bouguer gravity anomaly and elevation data. Knowing this, we can modify equation (6) to obtain subsidence  $y_1$  at location  $x_1 (= x_s - \delta)$  with reference to  $x_s$  as:

$$y_1 = \left( y_0 e^{-\pi/2} \right) e^{\lambda\delta} \sin \lambda\delta. \quad (8)$$

Here, knowing the width of the foreland basin  $\delta$ , flexural wavenumber  $\lambda$ , and the basement depth  $y_1$  at the mountain front, we can calculate maximum subsidence, load, etc. Assuming that the deflection is small compared to the wavelength of plate flexure, horizontal compressive stress ( $\sigma_x$ ) in the plate can be given by (Watts 2001)

$$\begin{aligned} \sigma_x(z) &= - \left( \frac{E}{1-v^2} \right) \frac{d^2 y}{dx^2} h(z) \\ &= - \left( \frac{2E\lambda^2}{1-v^2} \right) y_0 e^{-\lambda x} \sin \lambda x \, h(z). \end{aligned} \quad (9)$$

Here,  $h(z) = \pm T_e/2$ , is the depth coordinate for the elastic plate with the origin set at the middle with a positive axis pointing upward (figure S2, supplementary information). Negative sign represents extensional stress (Watts 2001). The vertical stress in the plate is expressed in terms of the horizontal stress as  $\sigma_z(z) = v\sigma_x(z)$ .

## 5. Datasets

For local intraplate stress computations, we have used topography and Bouguer gravity anomaly (BGA) data of the grid shown in figure 3. The grid covers the ADFB, the DSZ, the inferred DSR, and a part of the foreland basin north of the DSR. Elevation data were extracted from the Shuttle Radar Topography Mission (SRTM) data (Reuter *et al.* 2007; <http://srtm.csi.cgiar.org>) for the grid (69–82°E, 22–32°N). As we do not need very high-frequency data for local stress

computations, the raw SRTM data were low-pass filtered by using a Gaussian 3-point filter and then resampled at every 40th sample in both coordinate directions (figure 3a). These data were then rotated 45° counterclockwise so that the NE-trending ADFB becomes N–S (figure 3b). We extracted the grid (69–75, 26–32; rotated coordinate system) from the rotated data for use as the input for local stress computation. Similarly, the BGA grid was prepared from the 5 mGal contour map of India (GSI-NGRI 2006; <http://bhukosh.gsi.gov.in/Bhukosh/Public>). The central and northwestern parts of the figure is dominated by NE–SW trending BGA, whereas the trend changes in the northern part of the figure with the NW–SE trending contours of negative BGA caused by the flexure of the Indian plate (figure 3c). The grid rotation, same as for the SRTM data, was performed to get the BGA grid in the rotated coordinate system (figure 3d). Both datasets were sampled to get 128 × 128 grid of the input datasets for local stress computations.

## 6. Results

### 6.1 Local stresses

The elevation and the BGA datasets of the region enclosed in the white box marked in figure 3(b, d) are used to compute local stresses using the formulation presented in section 4.1. The values of the physical properties of various layers are listed in table 1. The Young's modulus ( $E$ ) can be estimated from seismic  $P$ -wave velocity ( $V_P$ ) and density ( $\rho$ ) of various rocks using the relationship  $E = \rho V_P^2 (1+v)(1-2v)/3v$ , where  $v$  is Poisson's ratio (Pauselli and Federico 2003). Similarly, Lame's parameters can also be calculated by using the relationship  $\lambda = Ev/\{(1+v)(1-2v)\}$  and  $\mu = E/\{2(1+v)\}$ . The load at the free surface due to topography is calculated as  $P_s = \rho_T gh$ , where  $\rho_T$  is the density of topography load, taken as 2600 kg/m<sup>3</sup>, and  $h$  is the elevation with respect to the free surface. The density of the asthenosphere is assumed to be 3100 kg/m<sup>3</sup>. The subsurface load ( $P_i$ ) at the  $i$ th interface due to mass heterogeneities is estimated from the BGA as  $P_i = (\rho_{i+1} - \rho_i)gh_i = B_a g/(2\pi G)$ , where  $G$  is the Gravity constant (Mandal *et al.* 1997). For  $B_a$  in mGal and load in MPa,  $P_i \cong B_a/4.19$ .

For obtaining a solution in the Fourier domain, the elevation and the BGA data have been

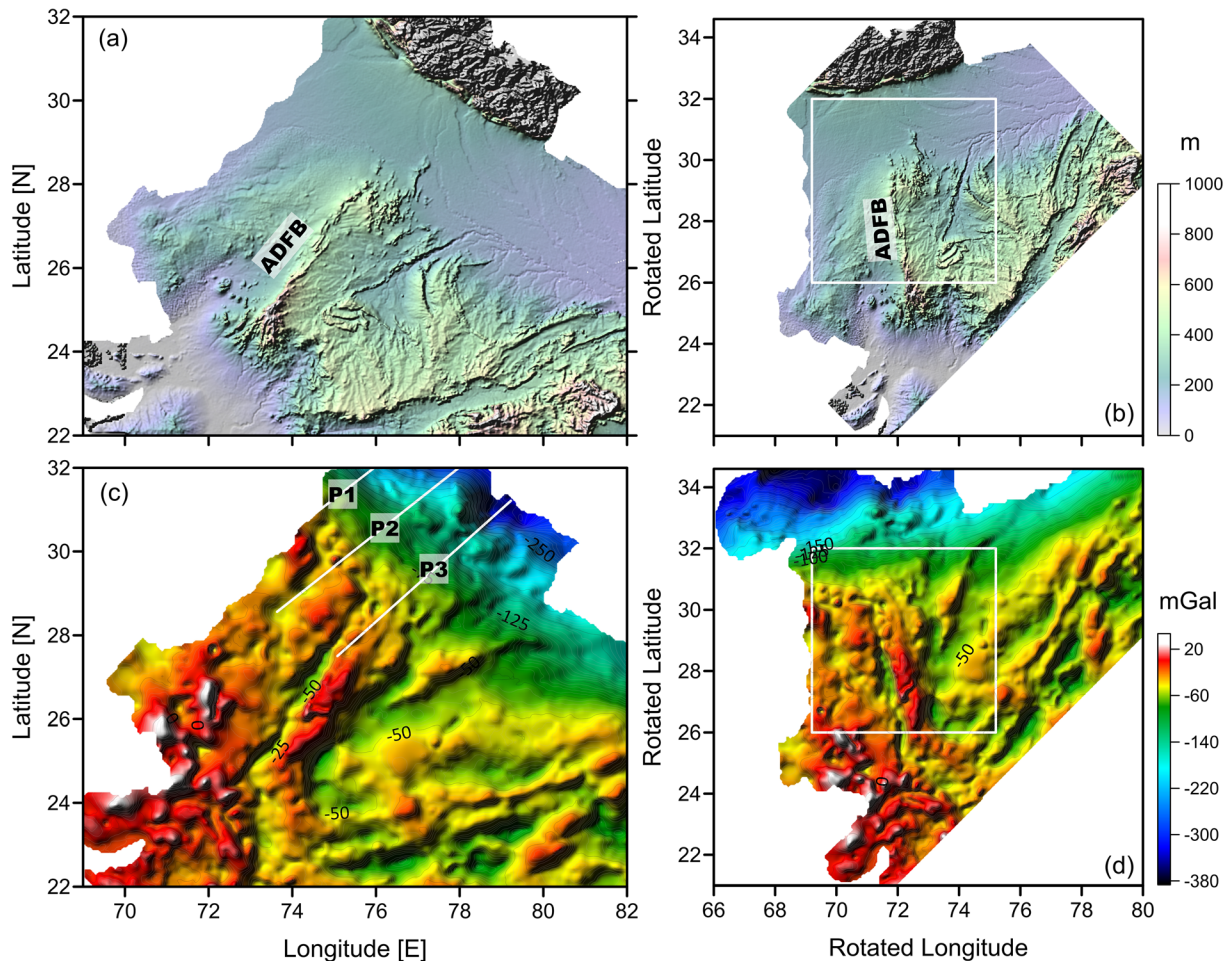


Figure 3. (a) Low-passed SRTM and (c) Bouguer gravity anomaly images of NW India. These are rotated 45° anticlockwise and shown in (b) and (d), respectively. White lines in 'c' are the profiles of LCM85 and white rectangular box in 'b' and 'd' is the domain used for local stress computations.

transformed into the Fourier domain. In order to distribute the load due to density heterogeneities on different interfaces, the Fourier power spectrum approach has been used to identify depth to the top of different interfaces from gravity and magnetic data. Dwivedi *et al.* (2019) used this approach and obtained a 3-layered crustal structure for this region. The depths of these layers are given in table 1. In their model, the wavenumbers corresponding to these layers are 0.09–0.03, 0.03–0.1 and <0.005 km<sup>-1</sup> for the basement, upper crust, and lower crust, respectively. For our grid of 6° × 6°, the minimum wavenumbers in the longitude (*x*-) and latitude (*y*-) directions are  $k_{\min}^x = 0.00086 \text{ km}^{-1}$  and  $k_{\min}^y = 0.00076 \text{ km}^{-1}$ , respectively, which gives the minimum radial wavenumber  $k_{\min}^r = 0.001148 \text{ km}^{-1}$ . For this radial wavenumber, the range of wavenumbers of various layers corresponds to grid numbers 78–26, 26–9, and 5–1, respectively. However, in order to avoid

very high-frequency content in the data due to the near-surface sources leading to instabilities when downward continued, we have restricted the highest wavenumber to the grid value of 64. Thus, the internal load is segregated to the basement, upper crust/lower crust interface, and the Moho load, assuming that the small wavelength load is of shallow origin and the large wavelength load is concentrated at progressively deeper levels.

The results of local stresses due to the topography and heterogeneities in the crustal density and mechanical properties at different depths are shown in figure 4(a). It can be seen that the amplitude of the shear stresses is small at 5 km depth, but from 10 km depth onwards, a large concentration of large shear stresses is obtained in the NE direction along the ADFB and in the NW direction along the DSR and the Ganga Basin. Between 10 and 25 km depth, the pattern of the

Table 1. Values of the physical and mechanical properties of various layers (Manglik et al. 2009).

Layer	Seismic velocity	Density	Depth of layer (km)	Young's modulus	Poisson ratio	Lame's parameters	
	$V_p$ (km/s)	$\rho$ (kg/m <sup>3</sup> )		$E$ ( $\times 10^{10}$ Pa)	$\nu$ ...	$\lambda$ ( $\times 10^{10}$ Pa)	$\mu$ ( $\times 10^{10}$ Pa)
Rocks above basement (assumed)	5.5	2500	2.9	6.302	0.25	2.521	2.521
Upper crust	5.75	2670	9.3	7.356	0.25	2.943	2.943
Lower crust	7.2	2900	40	12.88	0.25	5.151	5.151
Sub-Moho lithosphere	8.4	3350	100	19.70	0.25	7.879	7.879

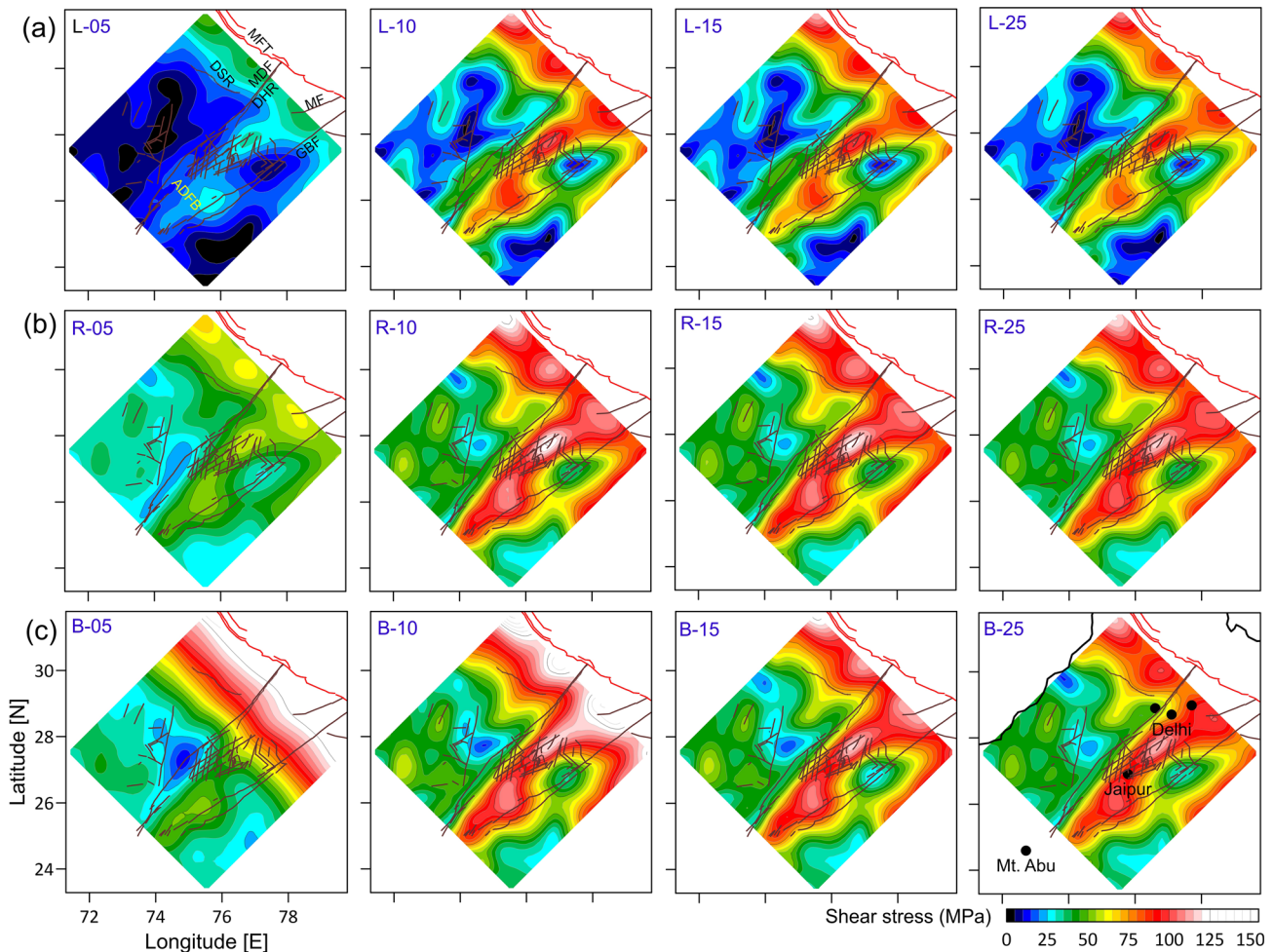


Figure 4. (a) Local shear stresses 'L' due to topography and crustal density and mechanical properties heterogeneities at 5, 10, 15, and 25 km depths; (b) shear stresses 'R' after the addition of regional NNE oriented  $SH_{max}$  of 50 MPa to the local stresses; and (c) shear stresses 'B' after the addition of plate bending stresses to the shear stresses shown in 'b'. Tectonic fabric of the region is superimposed on all figures and the names of major tectonic units are mentioned in the first figure.

large stress concentration remains very similar, with minor changes in the amplitude of the shear stresses. This implies that at shallow depths, the density heterogeneities at the basement level (2.9 km depth) do not have significant effect on the

generation of large intraplate stresses. However, the density and mechanical property heterogeneities at the upper crust/lower crust interface and at the Moho lead to the generation of large stresses in the region. Another significant feature of

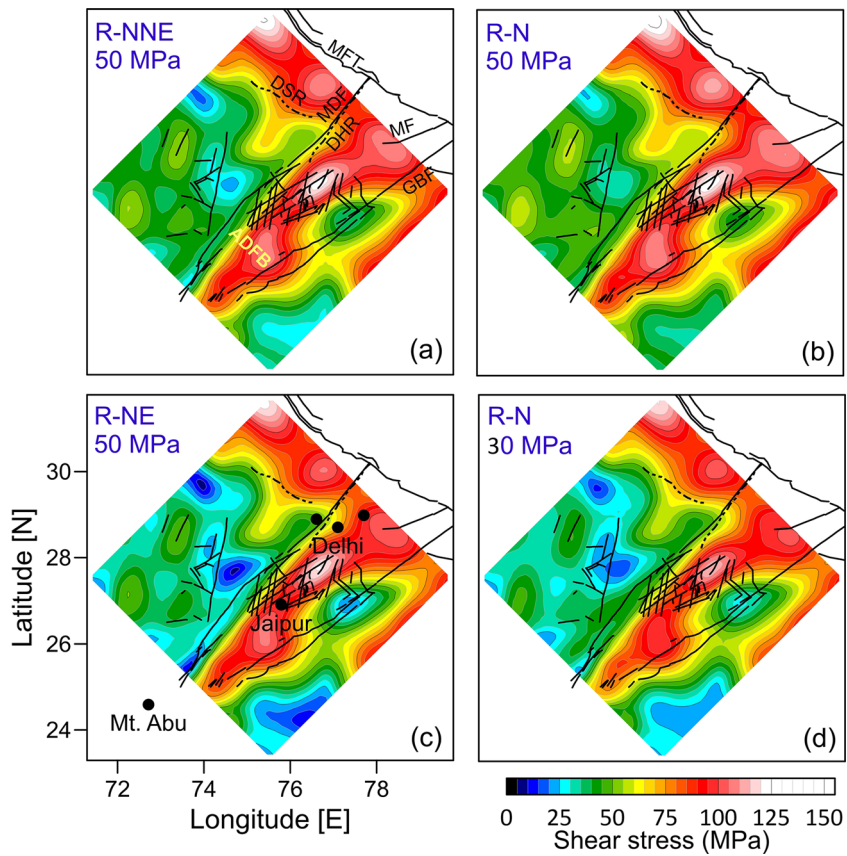


Figure 5. Effect of change in the direction of  $SH_{\max}$  on the pattern of total shear stress. (a) NNE, (b) North, and (c) NE. In these results, amplitude of  $SH_{\max}$  is 50 MPa. (d)  $SH_{\max}$  amplitude 30 MPa and direction North. Tectonic fabric of the region is superimposed on all figures and the names of major tectonic units are mentioned in the first figure.

the results is the presence of sharp gradients in the shear stresses, which could be considered as locales for intraplate seismicity.

## 6.2 Stress state with plate tectonic compressive stress

Next, we add regional compressive stress due to plate boundary forces to the computed local stresses to obtain the total stress distribution. The *in-situ* stress measurements within the Indian shield region suggest that the dominant direction of maximum horizontal compression,  $SH_{\max}$ , over the mid-continent region varies from N10°E to N40°E (Gowd *et al.* 1992; Heidbach *et al.* 2018). Mandal *et al.* (1997) suggested that a regional compressive direction of N10°E added to the local stresses yields the desired stress concentration needed to explain the Killari (Mb 6.9, 1993-09-29) intraplate earthquake in the Indian peninsular shield. Considering these estimates, we have added an NNE-oriented regional compressive stress of 50 MPa to the local stresses, and the results are shown

in figure 4(b). Stress measurements provide good estimates of the direction of  $SH_{\max}$ , but the magnitude remains poorly constrained. Our choice of 50 MPa is a bit ad-hoc, but tectonic stresses due to plate boundary forces are in a similar range (Zang and Stephansson 2010). In a later discussion, we analyze the effect of this parameter on stress generation. The results reveal that the regional stress direction is favourably oriented in the present case. Inclusion of regional stress to the local stresses only raises the amplitude of the resulting maximum shear stress in the region without significantly altering the pattern of shear stress distribution.

We further analyze the effect of the direction and amplitude of  $SH_{\max}$  on the stress state of the region. In figure 5(a), we show the maximum shear stress when  $SH_{\max}$  of 50 MPa is oriented in the NNE direction. This is compared with the stress state when the  $SH_{\max}$  direction is changed to N-S (figure 5b) and to NE-SW (figure 5c). The broad pattern of the stress state remains similar in all these three cases. The main difference is seen only in terms of the amplitude of the total shear stress. As we rotate  $SH_{\max}$  clockwise from N to NE, the

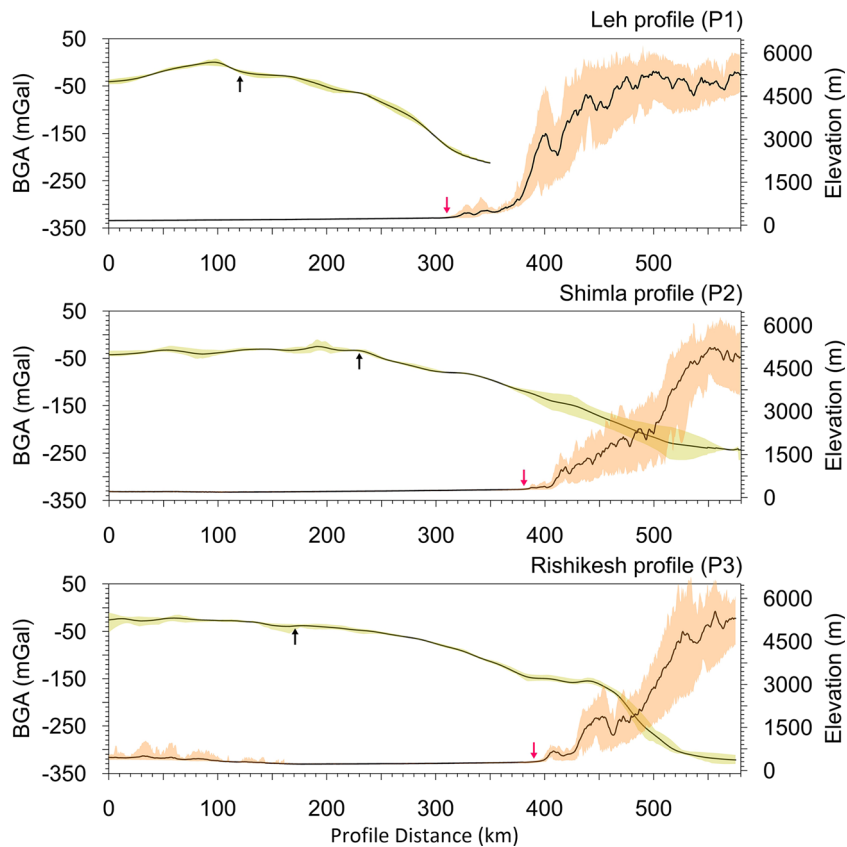


Figure 6. Variations of the elevation and the Bouguer gravity anomaly along the profiles of LCM85 across the Ganga Basin. Shaded regions are the minimum and maximum bounds for the swatch window of 25 km. Black arrows correspond to the initiation of plate flexure and red arrows represent the foothill region of the Himalaya. The locations of the profile are shown in figure 3.

amplitude of the shear stress changes without any noticeable change in its pattern with more pronounced patches of low shear stress in the case of N–S oriented  $SH_{\max}$ . We have also analyzed the effect of change in the amplitude of  $SH_{\max}$  on the computed shear stresses by reducing the amplitude to 30 MPa (figure 5d). It only affects the amplitude and not the pattern of the stress state. Thus, for our results, the amplitude and orientation of  $SH_{\max}$  do not have any primary effect in changing the pattern of the shear stress distribution.

### 6.3 Stress state after including plate bending stresses

The northern part of the study region is constituted of the Ganga Basin, which is formed due to the flexure of the Indian plate underthrusting the Himalaya. The forebulge of this flexure as well as the first node ( $X_S$ , figure S2, supplementary information) fall within our grid. The DSR may be considered as the axis of this forebulge based on the change in the Bouguer gravity anomaly from +ve value south of it to –ve value north of it (figure 3c).

Therefore, it is expected that the bending stresses could significantly influence the stress state of the region. Bilham *et al.* (2003) suggested that the flexure of the Indian lithosphere as it underthrusts the Tibetan Plateau can cause sufficient stresses in the flexural bulge region of central India as far as 670 km from the collision front leading to intraplate earthquakes in this region. Therefore, we explore the possible role of the plate bending stresses in modifying the stress state of the DSZ under the assumption of linear elasticity. There are several studies using gravity anomaly and elevation profiles across the Indian shield and the Himalaya to estimate the flexural rigidity and elastic thickness of the Indian plate and their variations along the Himalayan arc (e.g., Karner and Watts 1983; Lyon-Caen and Molnar 1983, 1985; Jordan and Watts 2005; Hetényi *et al.* 2006). Among these, we focus on three profiles of Lyon-Caen and Molnar (1985) (hereinafter referred as LCM85), two of which partly fall in our study area (figure 3). The Bouguer gravity anomaly and the elevation along these profiles extracted from figure 3 using 25 km swatch window are shown in figure 6. The model parameters and the values of the

Table 2. Values of control parameters used by Lyon-Caen and Molnar (1985) for flexural modeling. Profiles are marked in figure 3(c).

Profile	Unit	Mandi-Leh (P1)	Shimla (P2)	Rishikesh (P3)
Distance from the foothills Higher Himalaya topography rise ( $X_0$ )	km	$100 \pm 20$	$70 \pm 20$	$100 \pm 30$
Distance from the foothills to plate break ( $X'_0$ )	km	200	240	230
Flexural rigidity in the shield area ( $D$ )	Nm	$(0.3\text{--}0.5) \times 10^{24}$	$(2\text{--}4) \times 10^{24}$	$(0.5\text{--}2) \times 10^{24}$
Flexural rigidity beneath the Higher Himalaya ( $D'$ )	Nm	$5 \times 10^{22}$	$3 \times 10^{22}$	$3 \times 10^{22}$
Force at plate end ( $F_0$ )	N/m	$3.4 \times 10^{12}$	$3.4 \times 10^{12}$	$4 \times 10^{12}$
Plate bending moment ( $M_0$ )	N	$3.6 \times 10^{17}$	$3.5 \times 10^{17}$	$4 \times 10^{17}$
Basement depth at the foothills	km	–	3.0	3.5
Width of the Ganga Basin	km	–	–	220
Young's modulus	N/m <sup>2</sup>	$1.6 \times 10^{11}$	$1.6 \times 10^{11}$	$1.6 \times 10^{11}$
Density of lithosphere ( $\rho_m$ )	kg/m <sup>3</sup>	3300	3300	3300
Density of sediments ( $\rho_s$ )	kg/m <sup>3</sup>	2400	2400	2400

flexural rigidities fitting the Bouguer gravity anomaly for these profiles, obtained in LCM85, are given in table 2.

In LCM85, a two-layered model for the Indian plate consisting of the crust and the mantle lithosphere with densities of 2800 and 3350 kg/m<sup>3</sup>, respectively, was considered, which undergoes flexure by the Himalayan load of density 2700 kg/m<sup>3</sup>. The density of the Ganga Basin sediments infilling the basin was taken as 2400 kg/m<sup>3</sup>. In this model, the Indian plate beneath the Higher Himalaya was assumed to be relatively weak with flexural rigidity about two orders of magnitude smaller than that for the shield region of the plate (table 2). Further, a bending moment was applied at the northern end of the plate in order to explain the Bouguer gravity anomaly data. The plate bending equation was solved numerically, and the results yielded the flexural rigidity of the order  $10^{24}$  Nm for the shield region of the Indian plate with profile P2 having flexural rigidity about a factor of 4 to 8 larger than the flexural rigidity of profile P3. Flexural rigidity of profile P1 was estimated to be much lower than that of P2 and P3. For these values of the flexural rigidity and Young's modulus (table 2), and the Poisson ratio of 0.25, the elastic plate thickness ( $T_e$ ) for the shield region is estimated to be 20–41 km for P3 and 41–82 km for P2.

Flexural modelling along three profiles passing through the western (Kumaun–Garhwal), central (central Nepal), and eastern (Bhutan) sectors of the Himalayan belt was subsequently carried out by Jordan and Watts (2005), who concluded that there are significant along-strike variations in the elastic thickness of the Indian plate. In their results, the central segment has  $T_e$  of 70 km,

whereas in the eastern segment, it is 30 km and in the western segment, it is 50 km. They further extended the 1-D flexural analysis to 2-D by following iterative flexure and gravity anomaly modelling technique and obtained a variation in the  $T_e$  from about 100 km beneath the foreland basin to about 40 km beneath the Himalayan load for the central segment of the Himalayan arc. Although the estimates of  $T_e$  obtained by the 1-D and 2-D approaches vary in terms of absolute values, these reveal a broader scenario that the central Himalayan foreland basin has a strong rigid block and the Indian plate in the eastern and western sectors is comparatively less rigid (Manglik 2015). In this study, the value of Young's modulus was  $10^{11}$  N/m<sup>2</sup>. For this value of Young's modulus, values of the  $T_e$  obtained for the western profile of Jordan and Watts (2005) ( $T_e = 50$  km) and the Rishikesh profile (P3) of Lyon-Caen and Molnar (1985) ( $T_e = 48$  km considering  $D = 10^{24}$  Nm) are in good agreement.

The above studies incorporated reduced flexural rigidity and additional forces to explain mainly the Bouguer gravity anomaly and topography in the Higher Himalaya and further north, but the effect within the shield region is not expected to be much stronger. Therefore, we have adopted a simple formulation of flexure of a semi-infinite plate due to a line load, with constraints of known basin depth at the foothills and location of the first node of flexure from the BGA, to estimate the bending stresses within the foreland basin and the ADFB covering the region shown in figure 3. In order to select appropriate values of the control parameters, e.g., flexural rigidity, we analyze the effect of the basin width ( $\delta$ ) and the basement depth at the

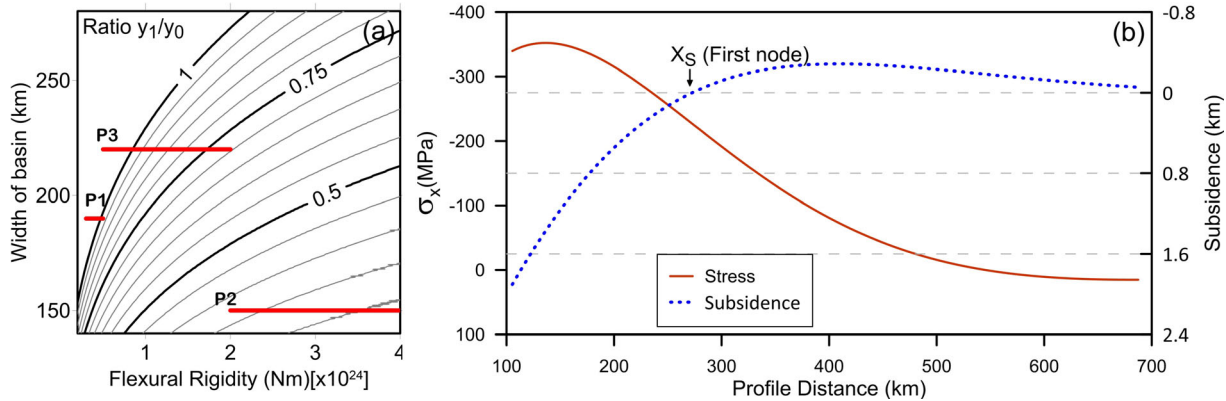


Figure 7. (a) Effect of basin width and flexural rigidity on maximum subsidence of a semi-infinite plate and (b) horizontal bending stress ( $\sigma_x$ ) on the top of the plate along the profile passing through the BGA grid (figure 3). Here, –ve sign represents extensional stress.

foothills of the Himalaya ( $y_1$ ) on the maximum subsidence ( $y_0$ ) using equation (3).

Figure 7(a) shows the effect of basin width and flexural rigidity ( $D$ ) on the maximum subsidence ( $y_0$ ) given the basement depth ( $y_1$ ) at the foothills. Profiles of LCM85 (table 2) are marked as red lines. Since  $y_1$  can not be more than  $y_0$  beneath the Himalayan collision belt, the curve corresponding to 1 is the limiting value. From this result, it can be seen that the values of the basin width and flexural rigidity obtained by LCM85 for profile P1 are not compatible. For P3 also, lower bound on  $D$  yields inconsistent results. However, the upper bound of this profile as well as the entire P2 yield  $y_0 > y_1$ . Since P3 passes through the ADFB and BGA high, we select the upper bound of  $D$  ( $2.0 \times 10^{24}$  Nm) for this profile, which is also consistent with the value of  $D$  for P2, and basin width of 220 km (figure 7). The basin depth at the foothills in the region is taken as 3 km (Lyon-Caen and Molnar 1985). Using these values, we get  $T_e \approx 55$  km for Young's modulus  $1.3 \times 10^{11}$  Nm $^{-2}$  and flexural wavenumber  $\lambda$  is  $0.0058$  km $^{-1}$ . For these control parameters, the horizontal bending stress at the top of the plate is calculated (equation (9) in supplementary information) and its variation with the profile distance within the study region is shown in figure 7(b). It can be seen that large extensional bending stresses at the top of the plate are present within the Ganga Basin. The amplitude of  $\sigma_x$  gradually decreases within our domain of stress computation.

#### 6.4 Combined stresses

The plate flexure profile is aligned approximately along the  $y$ -axis (general trend of the ADFB)

(figure 3c). Therefore, the bending stress varies only in this direction and there is no spatial variation along the  $x$ -direction. We have obtained maximum extensional bending stress of about 350 MPa in the northern segment of our grid covering a part of the Ganga Basin (figure 7b). The bending stress decreases in amplitude southward and becomes compressional in the southern segment of the grid. Within the plate, bending stress decreases linearly up to the neutral plane (figure 3) and then increases as compressional stress till the base of the elastic plate. The neutral plane is the plane of zero bending stress. Shear stress corresponding to the combined local, regional and bending stresses, denoted by 'B', for different depths is shown in figure 4(c). The results reveal that the bending stress has a significant influence on the intraplate stresses and the effect is depth dependent. For shallow depths (e.g., result for 5 km depth, figure 4c (first panel from left)), intraplate stresses are overwhelmed by the bending stress in the upper part of the elastic plate. In successively deeper slices, the influence of the bending stress reduces while the intraplate stresses dominate (figure 4c, right panel). This happens due to the decrease in the amplitude of the bending stress with depth up to the neutral plane. Such behaviour should manifest itself in terms of changes in the dominant mode of faulting.

#### 6.5 Fault mechanism solutions

Shear stresses give an idea about the zones of stress concentration. However, having computed the stress tensor, we can calculate the amplitude and orientation of the principal stresses and, thus, get

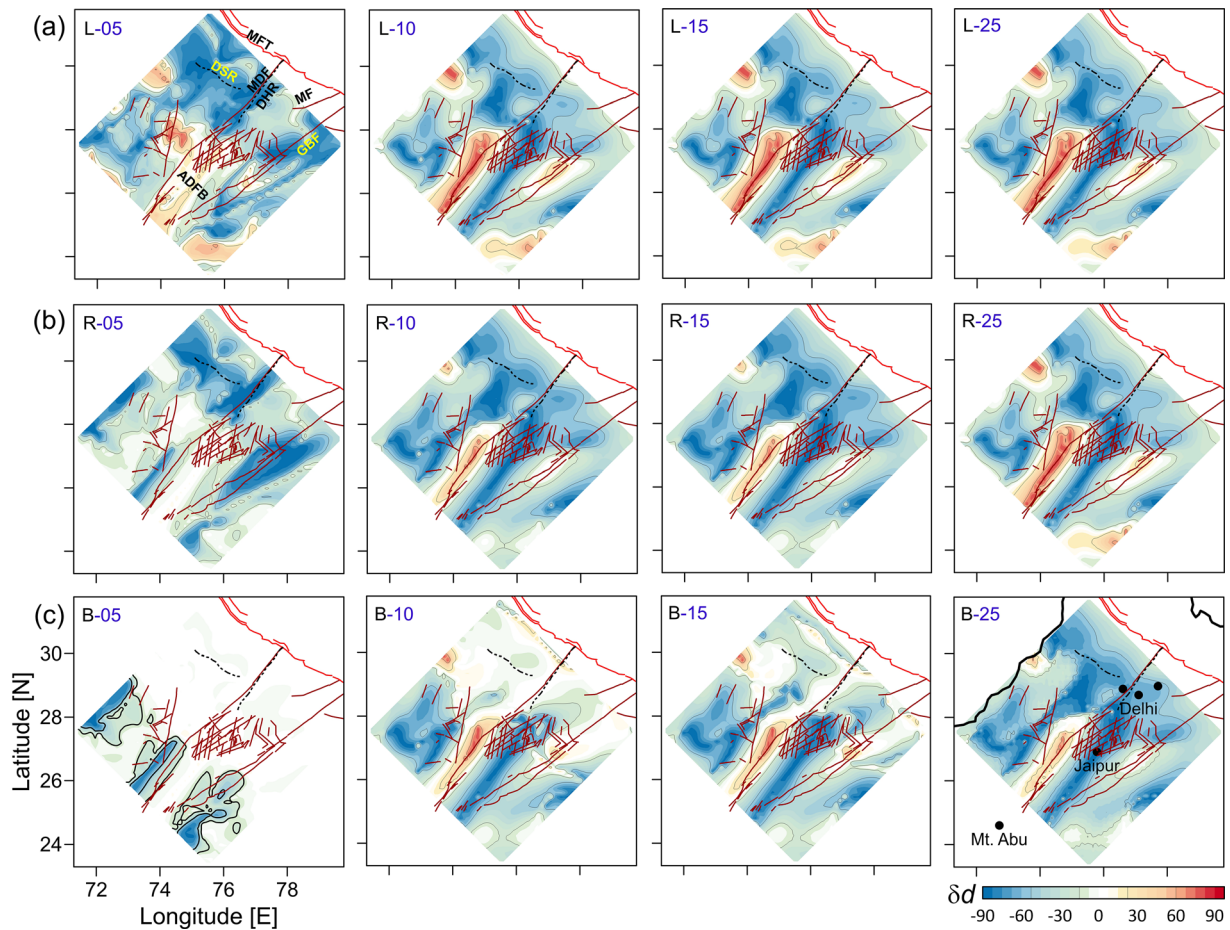


Figure 8. Variation of  $\delta d(\sigma_1^{\text{dip}} - \sigma_3^{\text{dip}})$  corresponding to the cases presented in figure 4. (a) Case of local intraplate stresses; (b) case with the addition of NNE oriented 50 MPa regional compressive stress; (c) same as 'b' but with the addition of bending stress. Tectonic fabric of the region is superimposed on all figures and the names of major tectonic units are mentioned in the first figure.

some idea about the feasible fault mechanism solutions corresponding to our results. We have calculated principal stresses and defined a parameter  $\delta d = \sigma_1^{\text{dip}} - \sigma_3^{\text{dip}}$ , the difference between the dips of maximum and minimum compressive stresses  $\sigma_1$  and  $\sigma_3$ , respectively. The value of  $\delta d$  varies between  $-\pi/2$  and  $+\pi/2$ . The ideal cases of  $\delta d = -\pi/2$ , 0, and  $+\pi/2$  represent thrust, strike-slip, and normal faulting, respectively. A value between these bounds indicates mixed-mode faulting mechanism. In the chosen colour code, blue region corresponds to dominant thrust faulting mechanism and red region is dominated by normal faulting mechanism. The white region has strike-slip mechanism. The results (figure 8a, b) support a dominant thrust environment over the entire crust down to 25 km except at 5 km depth, when only intraplate stresses (local as well as with the regional plate tectonic stresses) are considered. However, there are some prominent regions of

normal and strike-slip environment along the ADFB. At 5 km depth, several patches of normal faulting environment are obtained when only local stresses due to topography and heterogeneities in the crustal density and mechanical properties are considered (figure 8a). These change the strike-slip environment when regional plate tectonic stress is included in the local stresses (figure 8b).

A major departure from the results of dominant faulting mechanism due to intraplate stresses is seen when bending stress is included. For this case (figure 8c), we have obtained a dominant strike-slip environment at 5 km depth for almost the entire region, except for a few patches of thrust environment. When the bending stress is included, normal-type plate bending stress and thrust-type local stress (figure 8a) yield the resultant strike-slip mechanism (figure 8c). At 10 and 15 km depths, the region of strike-slip environment shrinks and paves way for the dominant thrust environment

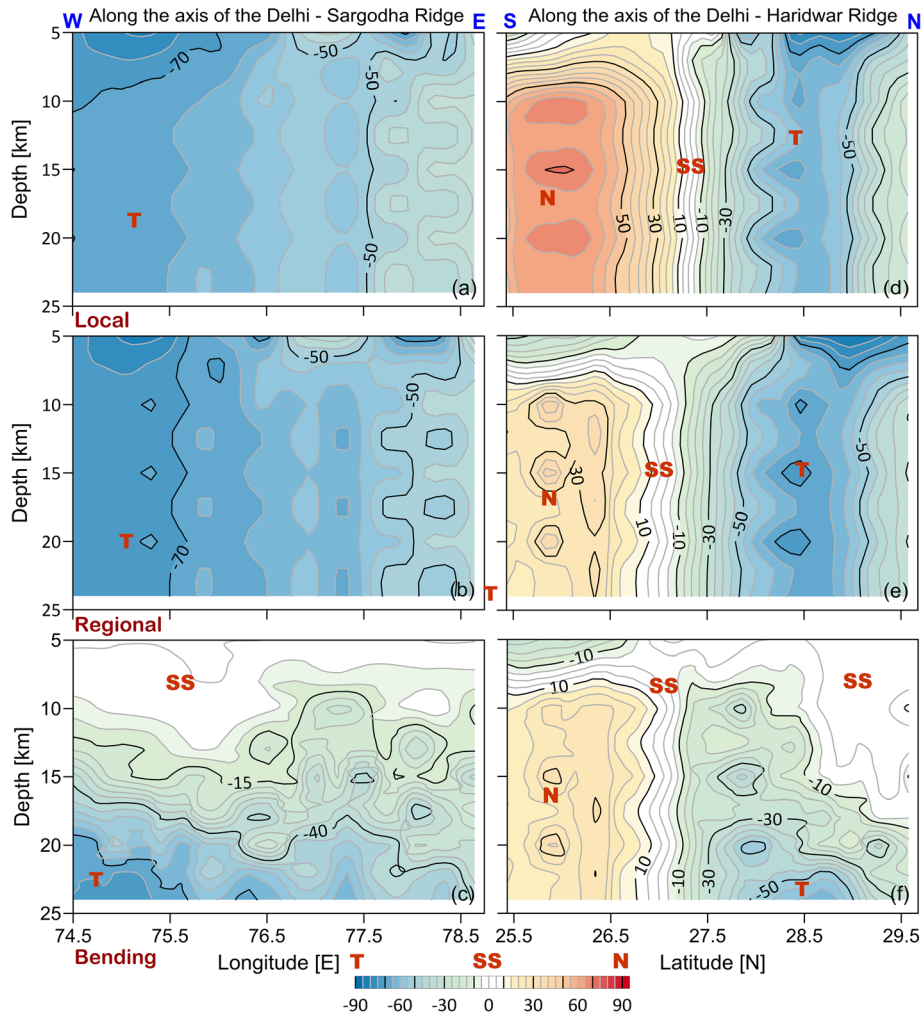


Figure 9. Depth sections of the variation of  $\delta d$ , a parameter representing the type of faulting mechanism, along the axis of the Delhi–Sargodha Ridge (DSR) (a, b, c) and the Delhi–Haridwar Ridge of the ADFB (d, e, f). The top, middle, and bottom panels represent local, regional, and bending stress cases, respectively. T: Thrust fault mechanism, SS: Strike-slip fault mechanism, and N: Normal fault mechanism.

with a minor zone of normal environment. Further deep, at 25 km depth, we get a dominant thrust environment. It can be seen that the strike-slip and thrust environments with a minor normal environment dominate along the ADFB, but along the DSR and in the Ganga Basin, only thrust environment dominates. Thus, our results suggest a significant variation in the faulting mechanisms, both spatially and with depth, in the region in the presence of bending stress that modifies the prevailing intraplate stresses due to topography and heterogeneities in the crustal density and mechanical properties and the regional plate tectonic stresses.

In figure 9, we present depth sections of the computed fault mechanisms along the DSR (figure 9a, b, c) and the ADFB (figure 9d, e, f). The top, middle, and bottom panels correspond to local, regional, and bending stress cases, respectively.

For the DSR, only local stresses and those with the addition of regional plate tectonic stresses support dominant thrust faulting mechanism, although the eastern part of the model domain yields thrust plus strike-slip environment. This scenario drastically changes when bending stresses due to the Indian plate flexure are included. Now, the upper 10 km is dominated by strike-slip mechanism and the thrust fault mechanism is dominated only below 20 km depth. The scenario is different for the ADFB where local and regional stresses subdivide the ADFB into three segments; the southern segment dominated by normal faulting mechanism, intermediate domain by strike-slip mechanism and northern part by thrust mechanism. In the presence of bending stresses, the pattern of computed faulting mechanisms changes drastically. Now, the upper 10 km is dominated by strike-slip mechanism and the regions of dominant normal and thrust

faulting support mix-mode faulting mechanisms. The northern part of the concealed ADFB (north of Delhi, 28.5–29.5N latitude) now has dominant strike-slip mechanism down to 15–20 km depth.

## 7. Discussion

We analyze the present stress modelling results in conjunction with the available focal mechanism solutions for the DSZ (table S1) to see if there is any correlation between the two datasets. Of the 27 events listed in table S1, eight have a magnitude  $\geq 3.5$ , 14 between 3 and 3.4, and 5 less than 3. Events of magnitude  $< 3$  occurred during 2007 and 2008. Irrespective of their magnitude, the events have been grouped into three depth ranges (0–10, 11–20, and 21–30 km) and plotted on the  $\delta d$  slices at 5, 15 and 25 km, respectively (figure 10). Our computations suggest a dominant strike-slip mechanism at 5 km depth for a majority of the DSZ region (figure 10a). Here, events 2, 15 and 17 have strike-slip behaviour with minor thrust components, which is broadly in agreement with our results of strike-slip environment. However, events 11 and 16 are thrust-type events, which do not match with our results. Event 11 has focal depth of 10 km, where thrust mechanism starts appearing (figure 8c, slice B-10). At the 15 km level (figure 10b), our results imply a progressive change from the strike-slip to the thrust environment for a majority of the DSZ region. However, there is a NE–SW oriented zone of strike-slip environment west of Delhi and many focal mechanisms fall in this region. The events such as 5 and 18 fall within the strike-slip region, whereas events 4, 10, 12, 13 and 14 are located in the mixed strike-slip and thrust environment. In this case, events 6, 8 and 9 ( $M_L \sim 3$ ) have dominant thrust components but fall in the strike-slip environment of our results.

Further deep at 25 km depth (figure 10c), events 1, 3 and 7 fall in the thrust-dominated environment with some mixing of the strike-slip environment. However, events 22, 25 and 26 showing normal faulting mechanisms are not explainable by our stress modelling results implying that some other process needs to be invoked to explain these normal faulting events. The fact that their magnitudes are very small ( $M_L \sim 2$ ) might warrant a re-look into their focal mechanisms as well. However, the 1966-08-15 (28.67N, 78.93E,  $M_w$  5.6) Moradabad earthquake (event number 27 in figure 2, and table S1 of supplementary information) within the

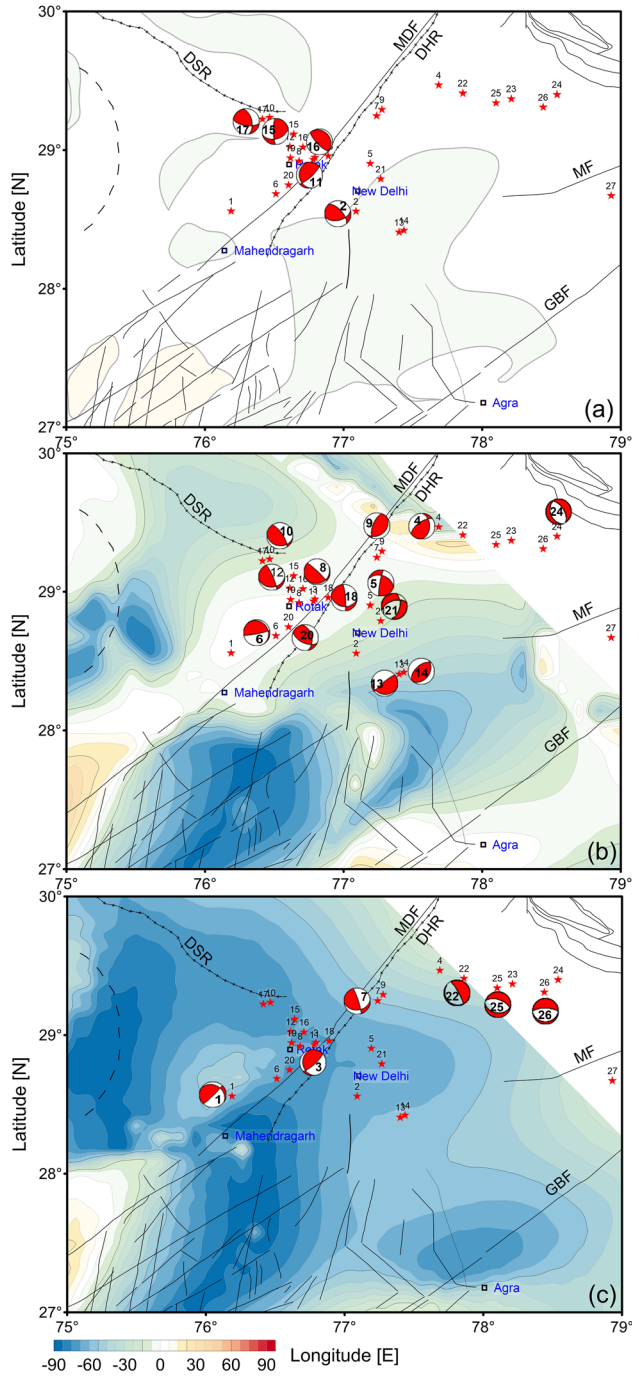


Figure 10. An enlarged view of  $\delta d$ , shown in figure 8(c), covering the Delhi Seismic Zone at three different depths (a) 5 km, (b) 15 km, and (c) 25 km. Focal mechanisms of earthquakes listed in table S1 (supplementary material) are also superimposed.

Ganga Basin also had a normal faulting focal mechanism (Molnar *et al.* 1973; Chouhan 1975). Copley *et al.* (2014) suggested that the normal faulting in the Ganga Basin is confined to the shallow (<20 km) depth beyond which thrust faulting dominates. They inferred that probably the bending of the Indian plate is leading to such a

change in the fault mechanism with depth. However, such an extensional stress state on the top of a plate is possible in the region of forebulge, which is further south of the epicentre of the earthquake. Between the topography load and the first node  $x_s = \pi/2\lambda$  (figure S2, supplementary information), the stress distribution will depend on the type of plate model used and the sediment load. Although the Moradabad event falls outside the domain of our computation, based on the present computations, we infer a strike-slip mechanism at shallow depths (figure 9a, b), but thrust-dominated mechanism at deeper levels (figure 9c). The presence of a major transverse tectonic feature segmenting the Indian plate (e.g., Valdiya 1976; Arora *et al.* 2012; Manglik *et al.* 2022b) and localized pore pressure effects could alter the stress regime of this region, which is not considered in the present model. Arora (1993) compared isostatic gravity anomaly, seismic shear wave velocity models and transverse electrical conductors by geomagnetic induction study and highlighted the difference in the crustal structures of the western and the eastern Ganga Basin. Such lateral variations in the crustal properties might alter the stress pattern. However, to study these effects, one needs to carry out full 3-D numerical stress modelling which is beyond the scope of the present study.

Thus, the contribution of the bending stresses, especially at depths <15 km is important to explain the occurrence of strike-slip earthquakes in the DSZ. In the absence of this component, the stress regime is dominated by thrust-faulting mechanism. We, therefore, infer that the stress regime of the intraplate DSZ due to local stresses arising from heterogeneities in the crustal density and mechanical properties and the regional compressive plate tectonic stress is modulated by regional plate bending stresses caused by flexing of the Indian plate by the Himalayan load. A combined effect of these stress components can explain the occurrence of both strike-slip and thrust earthquakes in the DSZ by virtue of it being located at the shoulder uplift region of the bending Indian plate. Bilham *et al.* (2003) and Vita-Finzi (2004) attributed the intraplate earthquakes in peninsular India to the forebulge region of the bending Indian plate. The effect of bending stress reduces away from the northern boundary of our study region with the decrease in the amplitude of the bending stress (figure 7b). We get a NE–SW trending belt aligned to the ADFB and having all three types of faulting mechanism behaviour. The normal

faulting zone, seen in the central part of the region (figure 10), gives way to strike-slip faulting behaviour in the southern part of the region. Thus, a large area of the southern ADFB (figure 1) is susceptible to strike-slip and thrust faulting mechanisms. In fact, many earthquakes around Mt. Abu have strike-slip focal mechanisms (figure 2) supporting our results.

The above results and the earthquake focal mechanisms suggest that the DSZ is not an intra-plate region in the classical sense of plate interior away from plate boundaries, rather, there is a coupling between the DSZ and the Himalayan collision belt. Such a coupling between the Delhi region and the Himalayan earthquakes has already been inferred based on the observations of damage of intensity VI on the Modified Mercalli intensity (MMI) scale in Delhi by the 1905 Kangra earthquake and shaking in this region by the 1991 Uttarkashi earthquake (Iyengar 2000). The effect of coupling between the intraplate DSZ and the Himalayan belt can be expected in two ways; inter-seismic change in the stress state of the DSZ during the seismic loading of active Himalayan mega-thrusts and co-seismic dynamic stress transfer from the Himalaya to the DSZ through the flexed Indian plate. Bilham *et al.* (2003) suggested another cause for temporal change in the stresses within the Indian plate in the form of time-varying flexural stresses due to continued northward convergence of the Indian plate. This mechanism implies that the faults within the intra-plate region also experience time-dependent loading, similar to that for plate boundary faults, as a consequence of time-varying flexural stresses. The co-seismic dynamic stress transfer from a Himalayan earthquake to the DSZ can take place in the form of a stress pulse through the flexed Indian plate, causing induced seismicity in the DSZ, which may not be instantaneous but may have a triggering delay (Belardinelli *et al.* 2003). The coupling between the Himalayan belt and the DSZ and the role of time-varying bending stresses, beside the local stresses, are additional important factors that should be considered while evaluating the comprehensive earthquake hazard assessment of the intra-plate DSZ and the northwest Indian shield.

## 8. Conclusions

The northwest Indian shield region experiences moderate level of intraplate seismicity along the NE–SW trending Proterozoic Aravalli Delhi Fold

belt (ADFB) and in a region encompassing Delhi and its surrounding region. The later seismicity is along the NNW to NW direction, coinciding with an inferred buried ridge extending from Delhi westward. The earthquakes along the ADFB are dominant of strike-slip nature, whereas those along the DSZ have both strike-slip and thrust-type focal mechanisms. Here, we have computed elastostatic local intraplate stresses due to heterogeneities in the physical and mechanical properties of crustal rocks and analyzed these in conjunction with the regional compressive plate tectonic stress due to the Indian plate convergence and bending stresses due to its flexure by the Himalayan load. The results suggest that the local crustal heterogeneities can induce significant intraplate stresses in the region. The NNE to NE oriented compressive plate tectonic stress, being favourably oriented to the strike of the ADFB, only amplifies the amplitude of local intraplate stresses without appreciably changing the pattern of the stresses. A major difference in the stress pattern is obtained when plate bending stresses due to the Indian plate flexure are added to the local stresses implying that the bending stresses possibly play an important role in regulating the stress state of the DSZ leading to earthquakes in the region having both strike-slip and thrust type focal mechanisms. We, thus, infer that the seismicity of the intraplate DSZ is influenced by the bending stresses generated in the Indian plate by the load of the Himalaya and conclude that its role should be considered together with local sources of stresses while evaluating the comprehensive earthquake hazard assessment of the intraplate DSZ and the northwest Indian shield.

## Acknowledgements

This research work was supported by CSIR-National Geophysical Research Institute (CSIR-NGRI) under the project MLP6404-28(AM). MDB received financial assistance from the project SSP801-28(AM) of CSIR-NGRI. The work has been approved by CSIR-NGRI for publication as contribution number NGRI/Lib/2021/Pub-84.

## Author statement

A Manglik: Conceptualization, methodology, computing, formal analysis, validation, writing – original draft, supervision. G Pavankumar:

Methodology, data curation, formal analysis, visualization, writing – original draft. M Demudu Babu: Data curation, formal analysis, visualization.

## References

- Arora B R 1993 Implications of electrical conductivity structures in the tectonic framework of northwest India; *Curr. Sci.* **64** 848–855.
- Arora B R and Mahashabde M V 1987 A transverse conductive structure in the northwest Himalaya; *Phys. Earth Planet. Int.* **45** 119–127.
- Arora B R, Gahalaut V K and Kumar Naresh 2012 Structural control on along-strike variation in the seismicity of the northwest Himalaya; *J. Asian Earth Sci.* **57** 15–24.
- Belardinelli M E, Bizzarri A and Cocco M 2003 Earthquake triggering by static and dynamic stress changes; *J. Geophys. Res.: Solid Earth* **108(B3)** 2135, <https://doi.org/10.1029/2002JB001779>.
- Bilham R, Bendick R and Wallace K 2003 Flexure of the Indian plate and intraplate earthquakes; *Proc. Indian Acad. Sci.: Earth Planet. Sci.* **112** 315–329.
- Braile L W, Keller G R, Hinze W J and Lidiak E G 1982 An ancient rift complex and its relation to contemporary seismicity in the New Madrid seismic zone; *Tectonics* **1**(2), 225–237.
- Carder D S 1945 Seismic investigations in the Boulder Dam area, 1940–1944, and the influence of reservoir loading on local earthquake activity; *Bull. Seismol. Soc. Am.* **35** 175–192.
- Chauhan P K S, Mohanty W K and Roonwal G S 1998 Earthquake hazards in area of low Seismicity: An example from NE Aravallis in Delhi region; In: *The Indian Precambrian* (ed) Paliwal B S, Scientific Publishers, pp. 523–530.
- Chouhan R K S 1975 Seismotectonics of Delhi Region; *Proc. Indian Nat. Sci. Acad.* **41(A)** 429–447.
- Copley A, Mitra S, Alastair Sloan R, Gaonkar S and Reynolds K 2014 Active faulting in apparently stable peninsular India: Rift inversion and a Holocene-age great earthquake on the Tapti Fault; *J. Geophys. Res.: Solid Earth* **119** 6650–6666, <https://doi.org/10.1002/2014JB011294>.
- Cox K 1989 The role of mantle plumes in the development of continental drainage patterns; *Nature* **342** 873–877.
- Dwivedi D, Chamoli A and Pandey A K 2019 Crustal structure and lateral variations in Moho beneath the Delhi fold belt, NW India: Insight from gravity data modeling and inversion; *Phys. Earth Planet. Inter.* **297** 106317.
- Gokarn S G, Rao C K and Singh B P 1995 Crustal structure in southeast Rajasthan using magnetotelluric techniques; In: Continental crust of northwestern and central India (eds) Gupta K R and Sinha-Roy S, *Geol. Soc. India Memoir* **31** 373–381.
- Gowd T N, Srirama Rao S V and Gaur V K 1992 Tectonic stress field in the Indian subcontinent; *J. Geophys. Res.: Solid Earth* **97** 11,879–11,888.
- GSI-NGRI 2006 *Gravity map series of India*; Geological Survey of India and National Geophysical Research Institute, Hyderabad, India.
- Heidbach O, Rajabi M, Cui X, Fuchs K, Müller B, Reinecker J et al. 2018 The World Stress Map database release 2016:

- Crustal stress pattern across scales; *Tectonophys.* **744** 484–498.
- Hetényi G, Cattin R, Vergne J and Nábělek J L 2006 The effective elastic thickness of the India Plate from receiver function imaging, gravity anomalies and thermomechanical modeling; *Geophys. J. Int.* **167** 1106–1118, <https://doi.org/10.1111/j.1365-246X.2006.03198.x>.
- Iyenger R N 2000 Seismic status of Delhi megacity; *Curr. Sci.* **78(5)** 568–574.
- Johnston A C and Kanter L R 1990 Earthquakes in stable continental crust; *Sci. Am.* **262(3)** 42–49.
- Jordan T A and Watts A B 2005 Gravity anomalies, flexure and the elastic thickness structure of the India–Eurasia collisional system; *Earth Planet. Sci. Lett.* **236** 732–750.
- Kamble V P and Chaudhary H M 1979 Recent seismic activity in Delhi and neighborhood; *Mausam* **30** 305–312.
- Karner G D and Watts A B 1983 Gravity anomalies and flexure of the lithosphere at mountain ranges; *J. Geophys. Res.: Solid Earth* **88(B12)** 10,449–10,477.
- Keiding M, Kreemer C, Lindholm C D, Gradmann S, Olesen O and Kierulf H P 2015 A comparison of strain rates and seismicity for Fennoscandia: Depth dependency of deformation from glacial isostatic adjustment; *Geophys. J. Int.* **202(2)** 1021–1028.
- Kuang J K, Long L T and Mareschal J-C 1989 Intraplate seismicity and stress in the southeastern United States; *Tectonophys.* **170** 29–42.
- Lilley F E M, Singh B P, Arora B R, Srivastava B J, Prasad S N and Sloane M N 1981 A magnetometer array study in northwest India; *Phys. Earth Planet. Inter.* **25** 232–240.
- Lyon-Caen H and Molnar P 1983 Constraints on the structure of the Himalaya from an analysis of gravity anomalies and a flexural model of the lithosphere; *J. Geophys. Res.: Solid Earth* **88** 8171–8191.
- Lyon-Caen H and Molnar P 1985 Gravity anomalies, flexure of the Indian plate, and the structure, support and evolution of the Himalaya and Ganga Basin; *Tectonics* **4(6)** 513–538.
- Mandal P, Manglik A and Singh R N 1993 Intraplate stresses along a section of Kavali–Udipi DSS profile of south Indian shield due to density heterogeneities and topography; *J. Geodyn.* **17** 203–211.
- Mandal P, Manglik A and Singh R N 1997 Intraplate stress distribution induced by topography and crustal density heterogeneities beneath the Killari, India, region; *J. Geophys. Res.: Solid Earth* **102** 11,719–11,729.
- Manglik A 2015 Thermo-mechanical structure of the Indian continental lithosphere; *J. Indian Geophys. Union* **19(3)** 243–255.
- Manglik A, Arora T, Thiagarajan S and Mallick A 2009 Intraplate Stresses due to crustal heterogeneities along the Nagaur–Jhalawar transect, northwestern India; *Curr. Sci.* **96** 838–843.
- Manglik A, Suresh M, Danda N, Pavankumar G, Demudu Babu M, Chakravarthi N N and Kandregula R S 2022a Subsurface expressions of the Aravalli–Delhi Fold Belt in the Western Ganga Basin by magnetotellurics; *J. Geol. Soc. India* **98** 1721–1727.
- Manglik A, Kandregula R S and Pavankumar G 2022b Foreland basin geometry and disposition of major thrust faults as proxies for identification of segmentation along the Himalayan Arc; *J. Geol. Soc. India* **98** 57–61, <https://doi.org/10.1007/s12594-022-1928-y>.
- Mareschal J-C and Kuang J 1986 Intraplate stresses and seismicity: The role of topography and density heterogeneities; *Tectonophys.* **132** 153–162.
- Mazzotti S, James T S, Henton J and Adams J 2005 GPS crustal strain, postglacial rebound, and seismic hazard in eastern North America: The Saint Lawrence valley example; *J. Geophys. Res.: Solid Earth* **110(B11)** 1–16.
- Mishra D C, Singh B, Tiwari V M, Gupta S B and Rao M B S V 2000 Two cases of continental collisions and related tectonics during the Proterozoic period in India – insights from gravity modelling constrained by seismic and magnetotelluric studies; *Precamb. Res.* **99** 149–169.
- Molnar P, Fitch T J and Wu F T 1973 Fault plane solutions of shallow earthquakes and contemporary tectonics in Asia; *Earth Planet. Sci. Lett.* **19** 101–112.
- Muir-Wood R 2000 Deglaciation seismotectonics: A principal influence on intraplate seismogenesis at high latitudes; *Quat. Sci. Rev.* **19(14–15)** 1399–1411.
- Pauselli C and Federico C 2003 Elastic modelling of the Alto Tiberina normal fault (central Italy): Geometry and lithological stratification influences on the local stress field; *Tectonophys.* **374** 99–113.
- Pavankumar G, Manglik A, Demudu Babu M and Chakravarthi N 2021 Magnetotelluric evidence for the presence of a deep electrical conductor in the vicinity of the Delhi Seismic Zone, India; *J. Earth Syst. Sci.* **130** 79, <https://doi.org/10.1007/s12040-021-01565-7>.
- Prakash R and Shrivastava J P 2012 A review of the seismicity and seismotectonics of Delhi and adjoining areas; *J. Geol. Soc. India* **79** 603–617.
- Rao M B R 1973 The subsurface geology of the Indo-Gangetic plains; *J. Geol. Soc. India* **14(3)** 217–242.
- Reuter H I, Nelson A and Jarvis A 2007 An evaluation of void filling interpolation methods for SRTM data; *Int. J. Geogr. Infor. Sci.* **21(9)** 983–1008.
- Roy A B 1988 Stratigraphic and tectonic framework of the Aravalli Mountain Range; In: Precambrian of the Aravalli mountain, Rajasthan, India (ed.) Roy A B, *Geol. Soc. India Memoir* **7** 3–31.
- Shukla A K, Prakash R, Singh R K, Mishra P S and Bhatnagar A K 2007 Seismotectonic implications of Delhi region through fault plane solutions of some recent earthquakes; *Curr. Sci.* **93(12)** 1848–1853.
- Simpson D W 1976 Seismicity changes associated with reservoir loading; *Eng. Geol.* **10** 123–150.
- Sinha-Roy S, Malhotra G and Guha D B 1995 A transect across Rajasthan Precambrian terrain in relation to geology, tectonics and crustal evolution of south-central Rajasthan; In: Continental crust of northwestern and central India (eds) Gupta K R and Sinha-Roy S, *Geol. Soc. India Memoir* **31** 63–89.
- Sykes L R 1978 Intraplate seismicity, reactivation of preexisting zones of weakness, alkaline magmatism, and other tectonism postdating continental fragmentation; *Rev. Geophys.* **16** 621–688.
- Tewari H C, Dixit M M, Rao N M, Venkateswarlu N and Vijaya Rao V 1997 Crustal thickening under the Paleo/

- mesoproterozoic Delhi Fold Belt in NW India: Evidence from deep reflection profiling; *Geophys. J. Int.* **129**(3) 657–668.
- Valdiya K S 1976 Himalayan transverse faults and folds and their parallelism with the subsurface structures of the north Indian plains; *Tectonophys.* **32** 353–386.
- Vita-Finzi C 2004 Buckle-controlled seismogenic faulting in peninsular India; *Quat. Sci. Rev.* **23** 2405–2412.
- Watts A B 2001 *Isostasy and flexure of the lithosphere*; Cambridge University Press.
- Zang A and Stephansson O 2010 *Stress field of the Earth's crust*; Springer, <https://doi.org/10.1007/978-1-4020-8444-7>.

Corresponding editor: GEORGE MATHEW